Peterson Peter K (Orcid ID: 0000-0002-9337-6677)
Nghiem Son V. (Orcid ID: 0000-0002-4592-2979)
Simpson William Robert (Orcid ID: 0000-0002-8596-7290)

Confidential manuscript submitted to Journal of Geophysical Research

Snow Melt Onset Hinders Bromine Monoxide Heterogeneous Recycling in the Arctic

Justine A. Burd[1], Peter K. Peterson[1,2], Son V. Nghiem[3], Don K. Perovich[4], and William R. Simpson[1*]

[1]Department of Chemistry and Biochemistry and Geophysical Institute, University of Alaska Fairbanks, Fairbanks, AK, USA

[2]Department of Chemistry, University of Michigan, Ann Arbor, MI, USA

[3]Jet Propulsion Laboratory, California Institute of Technology, Pasadena, CA, USA

[4]Cold Regions Research and Engineering Laboratory, Hanover, NH, USA

[*]Corresponding author: William R. Simpson (wrsimpson@alaska.edu)

Key Points:

- Snow melt onset hinders reactive bromine heterogeneous recycling and ends season of reactive bromine events.
- Reactive bromine events occur at sub-freezing air temperatures, but not at higher temperatures.
- Snow appears necessary for reactive bromine heterogeneous recycling, and rain water can terminate this chemistry.

This is the author manuscript accepted for publication and has undergone full peer review but has not been through the copyediting, typesetting, pagination and proofreading process, which may lead to differences between this version and the Version of Record. Please cite this article as doi: 10.1002/2017JD026906

Abstract

Reactive bromine radicals (bromine atoms, Br, and bromine monoxide, BrO) deplete ozone and alter tropospheric oxidation chemistry during the Arctic springtime (February – June). As spring transitions to summer (May – June) and snow begins to melt, reactive bromine events cease and BrO becomes low in summer. In this study, we explore the relationship between the end of the reactive bromine season and snow melt timing. BrO was measured by Multi-AXis Differential Optical Absorption Spectrometer (MAX-DOAS) at Utqiaġvik (Barrow), AK from 2012-2016 and on drifting buoys deployed in Arctic sea ice from 2011-2016, a total of 13 site/year combinations. The BrO seasonal end date (SED) was objectively determined and was compared to surface-air-temperature-derived melt onset date (MOD). The SED was highly correlated with the MOD (N=13, R^2 = 0.983, *RMS* = 1.9 days), and BrO is only observed at sub-freezing temperatures. In subsets of these sites/years where ancillary data was available, we observed that snowpack depth reduced and rain precipitation occurred within a few days of the SED. These data are consistent with snowpack melting hindering BrO recycling, which is necessary to maintain enhanced BrO concentrations. With a projected warmer Arctic, a shift to earlier snow melt seasons could alter the timing and role of halogen chemical reactions in the Arctic with impacts on ozone depletion and mercury deposition.

1 Introduction

Reactive bromine species (Br and its oxide form, BrO) are strong tropospheric oxidizers [*Platt and Hönninger*, 2003; *Simpson et al.*, 2007b, 2015; *Abbatt et al.*, 2012]. During Arctic springtime, enhanced BrO mixing ratios have been observed episodically up to ~40 pmol mol^{-1} [*Pöhler et al.*, 2010] as compared to levels found in the marine boundary layer of ~1-3 pmol mol^{-1} [*Leser et al.*, 2003] or ~1 pmol mol^{-1} in the free troposphere [*Theys et al.*, 2011]. Ozone normally dominates tropospheric oxidation by providing photooxidants, such as the hydroxyl radical [*Jacob*, 2000]; however, during springtime reactive bromine rapidly consumes ozone in ozone depletion events [*Bottenheim et al.*, 1986; *Oltmans and Komhyr*, 1986] and produces BrO [*Fan and Jacob*, 1992; *McConnell et al.*, 1992; *Hausmann and Platt*, 1994]. In addition, during ozone depletion events, reactive bromine rapidly oxidizes mercury from Hg^0 to Hg^{2+}, which gets subsequently deposited, becoming more bioavailable [*Schroeder et al.*, 1998; *Holmes et al.*, 2006, 2010; *Steffen et al.*, 2008]. As spring transitions to summer (i.e. late spring, May – June), however, observed BrO levels start decreasing and fewer ozone depletion events are observed [*Halfacre et al.*, 2014].

Snow-covered sea ice and low temperatures dominate springtime conditions in the Arctic Ocean. Also during springtime, satellite-based spectrometers (e.g. GOME, OMI, SCIAMACHY) detect BrO "hotspots" that occur primarily over frozen sea ice [*Richter et al.*, 1998; *Wagner and Platt*, 1998]. In late spring, the air temperature increases to above freezing and the snowpack starts melting, resulting in a sharp increase in the total snow melt extent across the Arctic sea ice surface in late May to early June [*Nghiem and Neumann*, 2007]. At approximately the same time

as snow melt, the satellite-detected BrO hotspots become less common, and they are essentially absent by June [*Van Roozendael et al.*, 2002]. Ground based observations of particulate bromine at Barrow, AK reported by *Berg et al.* [1983] showed enhanced particulate bromine levels (average 82 pptm, parts per trillion by mass) from February to April with decreasing values in May and very low levels (6 pptm) in June. In addition to observing BrO seasonality, ozone depletion events can be used as a proxy for enhanced BrO levels, due to the fact that reactive bromine catalytically destroys ozone. *Oltmans et al.* [1989] measured seasonal surface ozone at Igloolik, Barrow, Mould Bay, and Alert. The average behavior of ozone at Barrow had a winter maximum (November – February), decreased episodically in springtime (March – mid-May), and a secondary peak in June before decaying in summer [*Oltmans et al.*, 1989, 2012].

Current understanding of reactive bromine events in the Arctic [*Platt and Hönninger*, 2003; *Simpson et al.*, 2007b; *Abbatt et al.*, 2012] requires heterogeneous recycling of BrO to maintain reactive bromine levels. In the absence of recycling, reactive bromine species such as Br atoms would react with species such as formaldehyde (HCHO), producing HBr, which decreases reactive halogen levels, typically with a lifetime of a few hours. As proposed by chemical modeling groups [*Fan and Jacob*, 1992; *McConnell et al.*, 1992], the key chemical reaction for recycling is

$$HOBr + H^+ + Br^- \rightarrow (\text{on surface})\ Br_2 + H_2O. \qquad (1)$$

In addition to recycling reactive bromine, Reaction (1) is also central to the *bromine explosion* mechanism [*Platt and Janssen*, 1995; *Wennberg*, 1999] because it converts one inactive bromide (Br^-) ion to Br_2, which photolyses, releasing two reactive bromine atoms. Bromide, the inactive species of bromine, is found in sea salt and resides on surfaces such as frozen sea ice, frost flowers (vapor deposited crystalline structures), sea salt aerosols and snow throughout the Arctic [*Abbatt et al.*, 2012]. Two main requirements for BrO recycling are a high surface area to facilitate the reaction and the presence of bromide on those surfaces.

Laboratory studies have observed Reaction (1), on halide-doped frozen surfaces and found that more acidic surfaces were more efficient at producing Br_2 [*Huff and Abbatt*, 2002; *Wren et al.*, 2013]. This was verified in the field by *Pratt et al.* [2013], who examined reactive halogen production from a snow-chamber with snow and ice samples collected near Utqiaġvik, AK. They found that only the top 1 cm of the snowpack above both sea ice and tundra produced Br_2, when exposed to sunlight and ozone, as compared to sea ice and deeper snowpack layers. They also found that the top 1 cm of snow had a higher Br^-/Cl^- ratio and was more acidic, presumably due to atmospheric deposition of gas/particle-phase acids.

For near-surface BrO, snow is likely the predominant site for BrO recycling [*Simpson et al.*, 2007a; *Abbatt et al.*, 2012; *Pratt et al.*, 2013]. Measurements of Arctic snowpack surface area index (m^2 of snow per m^2 of ground) revealed the snowpack to have a very large surface area (up to 3000 $m^2\ m^{-2}$, [*Dominé et al.*, 2002]) compared to typical terrestrial soil or oceanic water. *Dominé et al.* [2002; 2011, 2012] classified snowpack layers and measured the surface

area of each layer during multiple Arctic field campaigns. Surface area measurements of Arctic snowpack layers revealed the top 1 cm of the snowpack to be generally surface hoar and/or diamond dust with an surface area index ranging from 50 – 120 m^2 m^{-2} and had lower total surface area compared to depth hoar (300 – 500 m^2 m^{-2}) and wind-packed layers (1000 – 2500 m^2 m^{-2}). The highest total surface area was measured in the wind-packed layers; however, these layers are very dense and less ventilated than surface and depth hoar layers [*Albert and Shultz,* 2002].

At the onset of snowpack melt, liquid water becomes present in snowpack, and there is a loss of surface area [*Dominé et al.*, 2002; *Taillandier et al.*, 2006; *Domine et al.*, 2007]. Ionselute downward inthe snowpack [*Johannessen and Henriksen*, 1978; *Bales et al.*, 1989], although capillary forces may retain melt water delaying ionic elution after melt onset [*Wever et al.*, 2014], and potentially redistribution of ions from atmospherically accessible surfaces to grain boundaries. Various studies have examined melt onset of snowpack in the Arctic [*Anderson*, 1987; *Winebrenner et al.*, 1994; *Kwok*, 2003; *Nghiem and Neumann*, 2007; *Markus et al.*, 2009]. *Kwok et al.* [2004] derived melt onset dates by Synthetic Aperture Radar satellite imagery and compared the melt onset dates against individual buoy temperature measurements from the International Arctic Buoy Program, as well as passive microwave brightness temperatures. They reported that melt onset occurred within 1-2 days of the buoy temperature crossing over 0˚C; however, the passive microwave brightness temperatures were biased towards a later melt stage. *Markus et al.* [2009] analyzed the minimum and maximum melt season length using the POLar Exchange at the Sea Surface (POLES) temperature data. The beginning of the maximum melt season, which coincided with the early melt onset date, was the first day the surface temperature increased to above freezing, independent of it staying above freezing. The objective of this study was to understand how environmental conditions associated with the onset of the late spring melt period affect BrO recycling. We used an extensive dataset, five spring seasons at Utqiaġvik, AK and eight spring seasons at on-sea-ice sites via O-Buoy measurements [*Carlson et al.*, 2010; *Knepp et al.*, 2010]. Where ancillary data were available, we explored the relationship between BrO abundance and environmental conditions such as temperature, snowpack depth, and precipitation (rain/snow).

2 Data sources and methods

2.1 Bromine monoxide measurement sites and methods

One MAX-DOAS instrument was located near Utqiaġvik, AK at the Barrow Arctic Research Center, BARC, (156.6679˚W, 71.3249˚N), where we used 2012 – 2016 data, which used a consistent observational pattern. MAX-DOAS instruments were also mounted on O-Buoy platforms that were deployed into Arctic Ocean sea ice from 2011 – 2016. Figure 1 shows a map of the O-Buoy locations, and Table 1 shows their coordinates on specific dates. O-Buoy instruments and deployments were a part of the National Science Foundation-funded Arctic Observing Network (AON) project. O-Buoys were designed for year-round measurement of

bromine monoxide, ozone, carbon dioxide, and meteorological variables such as temperature and wind [*Carlson et al.*, 2010; *Knepp et al.*, 2010]. O-Buoy deployments started in 2009 and a total of 15 O-Buoys have been deployed. Only a subset of deployed O-Buoy BrO measurements over the time range needed (April-June) for this study.

For the most straightforward comparison between these sites and years, we chose to use the directly measured BrO differential slant column density (dSCD), which was observed by Multi-AXis Differential Optical Absorption Spectroscopy (MAX-DOAS) [*Hönninger et al.*, 2004]. The dSCD is the difference in BrO column between a low elevation view, 1° elevation above the horizon, and the zenith, which is 90° elevation angle, and is most sensitive to boundary-layer BrO. While optimal estimation inverse modeling methods exist to convert dSCD profiles to vertical concentration profiles [*Frieß et al.*, 2011; *Peterson et al.*, 2015], these methods are complex, involve assumptions, and are sometimes numerically unstable. Of particular importance for this work, when observations of dSCD are near zero, the directly measured dSCD may be positive or negative, and the average accurately represents the observations. On the other hand, optimal estimation modeling only allows positive concentrations, so when BrO dSCDs are within noise levels of zero, the optimal estimation inversions contain a positive bias and the average may not correctly represent low BrO levels. Therefore, we chose to use simply the BrO 1° dSCD as a proxy for the presence or absence of BrO in the boundary layer. Enhanced BrO 1° dSCD measurements clearly indicate that BrO was present. Clouds, aerosol particles, fogs, and blowing snow can reduce visibility, which then reduces the differential pathlength between 1° elevation and zenith views and thus reduces the BrO 1° dSCD. Because reduced visibility periods are typically short lived (<day), visibility will have little effect on detecting the presence or absence of BrO on multi-day seasonal timescales. All BrO observations within ±0.5° of the nominal 1° elevation angle were averaged and the data were averaged over regularized 3-hour periods.

2.2 Snow / rain precipitation observations and snow depth measurements

Meteorological routine weather reports (METAR) at Utqiaġvik Airport (PABR, 156.7922˚ W, 71.2826˚ N) were used to determine snow and/or rain precipitation events. METAR derived from the US National Weather Service Automated Surface Observing System (NWS/ASOS) were obtained from the Iowa Environmental Mesonet (http://mesonet.agron.iastate.edu). Snow was indicated by the present weather code “SN” in more than one of the METAR observations in the 3-hourly averaging periods, and rain was indicated by the code “RA”, again in more than one METAR line. Snow depth was measured by Ice Mass Balance Buoys (IMB) [*Perovich et al.*, 2015]. An acoustic sounder was mounted on a pole frozen into the ice and positioned above the snow/ice surface. The acoustic sounder measured the distance between the instrument and the snow surface, with an accuracy of 5 mm, every hour, which was subsequently averaged to 3-hourly time resolution. Four O-Buoy-IMB seasonal comparisons were used in this analysis (refer to Table 1 for co-located instruments).

2.3 Objective determination of BrO termination and recurrence dates

Figure 2, top panels show BrO 1° dSCD from 20 April to 20 June on five consecutive years at Utqiaġvik. During this late season period, we observed that BrO began each season with high variability and values up to ~5 x 10^{14} molecules cm^{-2}. As the season progressed, each BrO record went through a transition where the BrO 1° dSCD became very small and scattered around zero. We call a date on which the BrO goes to zero a termination date. In some years, there is simply one termination date, but some years have a transient recurrence, where BrO is again non-zero, followed by a second termination date. We name the first termination date for a year the seasonal end date (SED).

We develop an objective algorithm to calculate termination and recurrence dates. This algorithm uses two parameters, the threshold below which BrO is considered zero, and the duration required for BrO to be under this threshold. The threshold is chosen to be $5x10^{13}$ molecule cm^{-2}, shown as a blue dashed horizontal line on each top panel of Fig. 2. The duration is chosen to be 5 days. The algorithm takes a termination date to be the last time when BrO 1° dSCD is above threshold such that not more than one 3-hour average is above threshold in the next 5 days. A recurrence is defined as the first point after a termination when BrO is above threshold and remains above threshold for more than one more data point for the next 5 days. If there is a recurrence, there will then be another termination. Blue dashed vertical lines on these figures show the objectively determined termination and recurrence dates. Note that in 2013, there was a data gap that coincided with an apparent BrO recurrence. Because we did not effectively capture this event's timing, we did not report this recurrence.

2.4 Objective determination of melt onset dates using surface air temperature

Air temperature at two meters above ground level in Utqiaġvik, AK near the BARC building was obtained from NOAA Earth System Research Laboratory Global Monitoring Division (http://www.esrl.noaa.gov/gmd/dv/data/). Air temperature measurements on the O-Buoy instruments were obtained from the arcticdata.io repository (http://arcticdata.io/). The O-Buoy temperature sensor was roughly 2-3 meters above the surface, depending upon snow depth and ice melt condition. All data are reported as 3-hour averages. Based on *Markus et al.* [2009] and *Kwok et al.* [2003], we defined the first date on which the temperature reaches 0˚C as the melt onset date (MOD), which is shown as a red-dashed vertical line

3 Results

Figures 2, 3 and 4, show BrO and temperature records, and visually indicate that the BrO termination dates were associated with warming above freezing. Because the temperature after the MOD often oscillates across freezing, we take the first date as the seasonal MOD, which is shown in Table 1 for each site/year. In some instances, we found that there were "early warming periods", as reported by *Winebrenner et al.* [1994], who detected snowpack melting using backscattering from European Remote Sensing 1 (ERS 1) SAR satellite imagery. They reported

that almost all melt onsets occurred when the temperature reached 0˚C; however, in one case they saw multiple periods where the temperature reached 0˚C before the melt onset date. They referred to these periods as "false start" of melting and explained that these short periods "did not lead to irreversible physical changes in those ice and snow properties that control backscattering at 5.3 GHz." Given that the literature indicates that these early melting periods exist, in five of the 13 cases, we chose to select a later warming above 0°C for the MOD. Notes in Table 1 describe these cases, and they will be discussed in section 4.1.Figure 5 panel (a) shows the relationship between MOD and SED is nearly 1:1. A linear regression analysis shows a strong correlation (R^2 = 0.983, N=13). The root mean square (RMS) of the difference between the SED and MOD (SED–MOD) for all sites/years was 1.9 days. The average bias of the difference between SED and MOD was -0.8 days. Figure 5 panel (b) shows the relationship between the BrO 1° dSCD and temperature, showing all valid data between 1 March and 3 July. This figure clearly shows that at sub-freezing temperatures, BrO 1° dSCD was highly variable between 0 and 8 x 10^{14} molecule cm^{-2}, but that upon warming above freezing, BrO 1° dSCD scattered around 0, indicating that BrO was absent above 0°C.

In four sea ice case studies, O-Buoy MAX-DOAS measurements were co-located with Ice-Mass Balance Buoys [*Perovich et al.*, 2015], which allowed for an ancillary study of snow depth in relation to SED. Figure 6, shows that snow depth was fairly constant prior to the SED (first blue dashed vertical line); however, the snowpack height typically began decreasing within a few days of the SED. During recurrence events, which occurred at O-Buoy10 and O-Buoy11 in 2015, panels (c) and (d), we observed that snow depth was stable.

Routine weather observations (METAR) at Utqiaġvik, AK allowed consideration of the weather relationship to the BrO end-of-season behavior. We observed that snow was quite common in this time of year, and rain became more common later in the season. In all years, rain events occurred within a few days of the seasonal end and recurrence dates. Also, we observed that during recurrences events, there was typically snow precipitation and not rain. In 2015, there was a transient rain event on 12 May, before the SED, but this event was followed by snow and then a more significant rain period after the SED on 20 and 21 May. In 2016, there were two brief freezing rain events, on 20 and 28 April that preceded the SED, but then a more extended rain period from 10-12 May after the SED.

4 Discussion

4.1 The seasonal end date is the melt onset date

Figure 5 panel (a) shows a strong correlation between SED and MOD. This finding is consistent with mid-season studies that indicate snowpack is a source of reactive halogen species and/or act as surface for recycling reactive halogens [*Simpson et al.*, 2007a; *Pratt et al.*, 2013]. The need for sufficient surface area is also indicated by studies of BrO aloft [*Frieß et al.*, 2011; *Peterson et al.*, 2017; *Simpson et al.*, 2017] that demonstrate enhanced aerosol surface area is

needed for BrO to be present aloft. The finding SED ≈ MOD is useful for predicting the end of the reactive halogen season. This is because satellite-based-methods developed for detection of melt onset [*Anderson*, 1987; *Winebrenner et al.*, 1994; *Kwok*, 2003; *Nghiem and Neumann*, 2007; *Markus et al.*, 2009] can be now extended to infer an end of the reactive bromine season. The end of BrO season behavior could then be used to validate satellite remote sensing of tropospheric BrO [*Theys et al.*, 2011; *Choi et al.*, 2012; *Sihler et al.*, 2012] on a Pan-Arctic scale.

The goal of the analysis here was to provide an objective means for determining SED and MOD to explore their relationship. However, we invoked literature to argue that some short warming events in five cases were not true melt onset dates. Therefore, it is useful to examine specific cases where either early melt onset was invoked or where the SED may not be perfectly determined by the objective algorithm. Figure 2, panel (b) shows Utqiaġvik 2013 data, which was a case where we used the 3rd date at which T>0°C as the MOD. We see that the earlier warming events (10 and 11 May) were associated with sub-threshold BrO, but the duration of the low BrO was not 5 days. This short duration caused the objective algorithm to not detect a SED during this warming. Had we manually selected this date as the SED, then there would have been recurrence event starting when the temperature drops and ending at the objectively-selected SED. Therefore, the data are consistent with the observation that the reactive halogen season terminates when the temperature goes above freezing. Each of the five cases (Utqiaġvik 2013 and 2015, O-Buoy2 2011, O-Buoy6, 2012, and O-Buoy10 2014) shows the same behavior as just discussed; the early melt event was associated with low BrO 1° dSCD that was either too short in duration (<5 days) or near threshold to be detected as the SED.

Another notable case is that of O-Buoy 14 in 2016, shown on Fig. 4, panel (d), which shows an early MOD followed by a later SED. The data show that at the time of the MOD, BrO undergoes a typical end-of-season transition to sub-threshold levels, but again the duration is too short for the objective algorithm to call this date the SED. If we were to manually adjust these cases, the agreement between MOD and SED could be improved. However, the selection of one of these dates would then be dependent on the other date, so the correlation would be automatic and thus meaningless.

It is also evident from examination of the in-season (before the SED) behavior of BrO that low levels of BrO 1° dSCD can occur for a few days. Therefore, the SED is uncertain by a few days because BrO could have been sub-threshold fortuitously, unrelated to snow condition, and we do not attempt to interpret the differences less than a few days. Similarly, past work has shown that MOD is not perfectly determined by temperature metric alone [*Winebrenner et al.*, 1994] but is significantly affected by infrared radiation budget and latent heat fluxes [e.g. *Vionnet et al.*, 2012], leading to the same caveat. Within this view of SED and MOD potentially having a few days uncertainty, we take the high correlation shown on Fig. 5(a) as excellent indication that the melt onset occurs within a couple days of the termination of the reactive bromine season.

4.2 BrO events occur up to freezing, but not at above-freezing temperatures

Figure 5 panel (b) clearly demonstrates that BrO events occur up to freezing temperatures, and not above freezing. Below freezing, there is a great deal of variability in BrO 1° dSCD, with an increase in the peak dSCD as the temperature decreases from 0°C to approximately -10°C and then a rather flat envelope. However, we note that the dSCD of BrO is an indicator for the detection of BrO, but not directly related to surface concentrations or the lower-tropospheric vertical column density of BrO. In the future, work using optimal estimation modeling from these data should assist in quantitatively determining the relationship between temperature and bromine activation. Using data from a subset of these years at Utqiaġvik and two O-Buoys, *Peterson et al.* [2015] found that the lower-tropospheric vertical column density of BrO was clearly enhanced at temperatures up to -5°C, in agreement with the analysis here on a more extensive data set. *Bottenheim et al.* [2009] showed that ozone depletion events, which are caused by reactive bromine chemistry, were observed at air temperatures up to -6˚C, providing indirect evidence that reactive bromine can occur close to freezing temperatures. On the other hand, *Pöhler et al.* [2010] found surface BrO mixing ratio decayed to zero as temperature increased to –15°C, a much colder threshold than we observe. However, the *Pöhler et al.* [2010] study occurred during the peak reactive bromine season in March – April 2009, and only ever experienced temperatures up to –15°C. The episodic nature of reactive bromine events could have caused low BrO mixing ratio in that short-term study, which was interpreted as a threshold. It is clear from the data presented in the current study that BrO is present at temperatures above –15°C, and in fact up to freezing.

4.3 Decaying snowpack and rain precipitation hinders BrO recycling

Figure 6 shows that periods of significant decrease in snowpack thickness are associated with sub-threshold BrO levels. Figure 6, panels (c) and (d) particularly show that after all of the termination dates (when BrO went below threshold), snowpack thickness was decreasing. This compaction of snowpack occurs via liquid water presence on snow grains, which causes coalescence and snowpack height decrease [*Colbeck*, 1982; *Brun*, 1989]. In one study, end of season compaction decreased the total surface area of a snowpack by an order of magnitude in a few weeks [*Taillandier et al.*, 2006]. In addition, the top of the snowpack may form a melt-freeze crust that has very little surface area [*Domine et al.*, 2007] and may significantly decrease the ventilation of the snowpack [*Albert and Perron*, 2000]. In addition to warming, rain water from precipitation would induce snowpack decay due to the increase of liquid water content. Figure 7 shows that rain water typically occurs within a few days after the BrO termination date. The Utqiaġvik 2016 case, shown on Fig.7(e) is interesting and unique in having two freezing rain events before the SED. During both of these events BrO is near to below threshold, consistent with either low surface area or decreased through-snow ventilation [*Albert and Perron*, 2000]. Note by comparing Fig. 2 panel (e) to the prior years (Fig. 2 prior panels) that BrO was lower during April 2016 than other years. Potentially 2016 could show the result of an earlier spring to

summer transition [*Stone et al.*, 2002; *Markus et al.*, 2009] as lower BrO during this transitional period due to earlier melting and freezing rain.

4.4 Below freezing temperatures and new surface area re-initialize BrO recycling

All recurrence events were associated with sub-freezing temperatures, as evident from Figs. 2-4. However, there were periods where the temperature was below freezing, but no recurrence event was observed. Key examples of sub-freezing periods that lack BrO are Utqiaġvik 7-11 May 2014 (Fig. 2(c)) Utqiaġvik 14-21 May 2016 (Fig. 2(e)), O-Buoy12 31 May – 14 June 2015 (Fig. 4(c)), and O-Buoy14 15-20 May 2016 (Fig. 4(d)). These periods indicate that simply being below freezing is not sufficient to regain the capacity to recycle BrO. From the cases at Utqiaġvik where recurrences did occur, 2012, 2014, and 2015, Fig. 7 (panels (a), (c), and (d), respectively) shows that snow precipitation preceded the recurrence events. It is likely that the recurrence in early June at Utqiaġvik in 2013 (Fig. 7(b)), which was not well captured due to a data gap, also fits this pattern of snow precipitation before BrO recurrence.

4.5 What property of snowpack is changed at the BrO season end?

Snow melt involves multiple coupled phenomena that confound interpretation of why the occurrence of snow melt is correlated with BrO season termination. When snow begins to melt, the surface goes from solid to liquid, and liquid surfaces have been shown to often have lower heterogeneous reactivity than solid ice [*Kahan et al.*, 2010a, 2010b; *Domine et al.*, 2013]. This diminished reactivity upon liquid surface formation can explain the rapid loss of BrO upon melting. However, we observe a number of cases (see section 4.4) where sub-freezing temperatures are experienced after melt onset, but the re-frozen snow does not recycle BrO. A possible explanation for these cases is that while in the surface-melted state, bromide (Br^-) ions could redistribute from atmospherically accessible snow surface locations to thermodynamically favored grain boundaries [*Baker et al.*, 2003; *Bartels-Rausch et al.*, 2014] or other locations that are less accessible for heterogeneous chemistry. Re-frozen and metamorphosed snowpack would have significantly lower surface area than fresh fallen snow [*Domine et al.*, 2007]. Similarly, a melt-freeze or freezing rain crust on top of snowpack would drastically decrease ventilation throughout the snowpack [*Albert and Perron*, 2000] and would reduce wind pumping that would allow for Br_2 to be released from the interstitial space of the snowpack [*Pratt et al.*, 2013]. Both the loss of surface area and hindered ventilation would slow BrO recycling, which is a potential cause in the termination behavior when the snowpack begins to melt. Another potential contributor to removal of bromide ions is the "ionic pulse" phenomenon [*Johannessen and Henriksen*, 1978; *Bales et al.*, 1989], which describes the observation of high ionic impurity concentrations in initial runoff from melting snow. However, actual percolation throughout the snowpack and runoff is likely to be a slower process than top surface melting, which would be inconsistent with the immediacy of BrO termination at MOD. Therefore, it seems more likely that decreased reactivity due to liquid surfaces, loss of surface area, and/or hindered ventilation would be responsible than extensive ion runoff. Which of these factors can be the most important

remain to be determined, but all lead to a similar effect – that BrO recycling is hindered upon snow melt. Laboratory and field manipulation studies that separate these coupled phenomena are encouraged to improve mechanistic understanding of reactive bromine recycling.

5 Conclusion

Melt onset, snowpack depth and rain/snow precipitation were investigated to understand their effects on BrO recycling. We objectively determined the seasonal end date (SED) to the reactive bromine season, as well as the temperature-based melt onset dates (MOD) for thirteen cases from Utqiaġvik, AK and O-Buoy observations from 2011 – 2016. The strong correlation of the SED occurring within a few days of the MOD indicates these phenomena are strongly coupled. Correlation of BrO abundance with temperature clearly shows that BrO is only present at sub-freezing temperatures, and also that BrO is above zero within a few degrees below freezing. From these observations, we find that melt onset hinders BrO recycling and ends the reactive bromine season. Ancillary snowpack depth analysis at sea ice sites revealed that the snow depth decreased within a few days of the SED and MOD, which supports that melt onset of the snowpack inhibits BrO recycling. Rain precipitation data at Utqiaġvik similarly showed the rain occurred a few days after the SED and suggests that again there is a loss of snowpack surface area due to liquid water, which is hindering BrO recycling. New snow precipitation observations at coastal sites revealed snow may be necessary to re-initialize BrO recycling but it is not sufficient alone.

The finding that the start of the melt onset season is the end to the BrO season, gives us an indication on how BrO may respond to future climate changes. Long-term studies on the summer melt season found that the melt season has lengthened ~8 days per decade for Utqiaġvik, AK [*Stone et al.*, 2002] and ~5 days for the pan-Arctic region [*Markus et al.*, 2009]. These summer melt trends and our results indicate that as the melt season lengthens, the BrO season will get shorter, which would reduce the amount of ozone depletion events and mercury deposition during late spring.

Acknowledgments and Data

The authors declare no financial conflicts of interest. The authors would like to thank Rick Thoman at NOAA (Fairbanks, AK), as well as Bruce Elder at CRREL (Hannover, NH) for advice and providing measurement data. We thank the reviewers, especially Dr. Florent Domine, for constructive comments. This research was supported by the Department of Chemistry and Biochemistry at University of Alaska Fairbanks, the National Aeronautics and Space Administration (NASA) Cryospheric Sciences Programs (CSP) and the National Science Foundation (NSF) under grant ARC-1602716. The research carried out at the Jet Propulsion Laboratory, California Institute of Technology, was supported by the NASA CSP under which the InterDisciplinary Science (IDS) research was implemented to successfully accomplish the

BROMEX field campaign. O-Buoy data are accessible from the NSF-funded http://arcticdata.io repository. Meteorological data sources are cited in text.

References

Abbatt, J. P. D. et al. (2012), Halogen activation via interactions with environmental ice and snow in the polar lower troposphere and other regions, *Atmos. Chem. Phys.*, *12*(14), 6237–6271, doi:10.5194/acp-12-6237-2012.

Albert, M. R., and F. R. Perron (2000), Ice layer and surface crust permeabilty in a seasonal snow pack, *Hydrol. Process.*, *14*, 3207–3214.

Albert, M. R., and E. F. Shultz (2002), Snow and firn properties and air–snow transport processes at Summit, Greenland, *Atmos. Environ.*, *36*(15–16), 2789–2797, doi:10.1016/S1352-2310(02)00119-X.

Anderson, M. R. (1987), The Onset of Spring Melt in First-Year Ice Regions of the Arctic as Determined From Scanning Multichannel Microwave Radiometer Data for 1979 and 1980, *J. Geophys. Res.*, *92*(13), 153–163.

Baker, I., D. Cullen, and D. Iliescu (2003), The microstructural location of impurities in ice, *Can. J. Phys.*, *81*(1–2), 1–9, doi:10.1139/p03-030.

Bales, R. C., R. E. Davis, and D. A. Stanley (1989), Ion elution through shallow homogeneous snow, *Water Resour. Res.*, *25*(8), 1869–1877, doi:10.1029/WR025i008p01869.

Bartels-Rausch, T. et al. (2014), A review of air-ice chemical and physical interactions (AICI): liquids, quasi-liquids, and solids in snow, *Atmos. Chem. Phys.*, *14*(3), 1587–1633, doi:10.5194/acp-14-1587-2014.

Berg, W. W., P. D. Sperry, A. Rahn, and E. S. Gladney (1983), Atmospheric Bromine in the Arctic, *J. Geophys. Res.*, *88*, 6719–6736.

Bottenheim, J. W., A. G. Gallant, and K. A. Brice (1986), Measurements of NO Y species and O 3 at 82° N latitude, *Geophys. Res. Lett.*, *13*(2), 113–116, doi:10.1029/GL013i002p00113.

Bottenheim, J. W., S. Netcheva, S. Morin, and S. V. . Nghiem (2009), Ozone in the boundary layer air over the Arctic Ocean: measurements during the TARA transpolar drift 2006-2008, *Atmos. Chem. Phys.*, *9*, 4545.

Brun, E. (1989), Investigation on wet-snow metamorphism in respect of liquid-water content, *Ann. Glaciol.*, *13*, 22–26.

Carlson, D., D. Donohoue, U. Platt, and W. R. Simpson (2010), A low power automated MAX-DOAS instrument for the Arctic and other remote unmanned locations, *Atmos. Meas. Tech.*, *3*(2), 429–439, doi:10.5194/amt-3-429-2010.

Choi, S. et al. (2012), Analysis of satellite-derived Arctic tropospheric BrO columns in conjunction with aircraft measurements during ARCTAS and ARCPAC, *Atmos. Chem. Phys.*, *12*(3), 1255–1285, doi:10.5194/acp-12-1255-2012.

Colbeck, S. C. (1982), An overview of seasonal snow metamorphism, *Rev. Geophys.*, *20*(1), 45, doi:10.1029/RG020i001p00045.

Domine, F., A.-S. Taillandier, and W. R. Simpson (2007), A parameterization of the specific surface area of seasonal snow for field use and for models of snowpack evolution, *J. Geophys. Res. Surf.*, *112*(F2), doi:10.1029/2006JF000512.

Domine, F., J.-C. Gallet, M. Barret, S. Houdier, D. Voisin, T. A. Douglas, J. D. Blum, H. J. Beine, C. Anastasio, and F.-M. Bréon (2011), The specific surface area and chemical composition of diamond dust near Barrow, Alaska, *J. Geophys. Res.*, *116*, D00R06, doi:10.1029/2011JD016162.

Domine, F., J.-C. Gallet, J. Bock, and S. Morin (2012), Structure, specific surface area and thermal conductivity of the snowpack around Barrow, Alaska, *J. Geophys. Res. Atmos.*, *117*(D14), n/a-n/a, doi:10.1029/2011JD016647.

Domine, F., J. Bock, D. Voisin, and D. J. Donaldson (2013), Can We Model Snow Photochemistry? Problems with the Current Approaches, *J. Phys. Chem. A*, *117*(23), 4733–4749, doi:10.1021/jp3123314.

Dominé, F., A. Cabanes, and L. Legagneux (2002), Structure, microphysics, and surface area of the Arctic snowpack near Alert during the ALERT 2000 campaign, *Atmos. Environ.*, *36*(15–16), 2753–2765, doi:10.1016/S1352-2310(02)00108-5.

Fan, S.-M., and D. J. Jacob (1992), Surface ozone depletion in Arctic spring sustained by bromine reactions on aerosols, *Nature*, *359*, 522–524.

Fetterer, F., M. Savoie, S. Helfrich, and P. Clemente-Colón. (2010), Multisensor Analyzed Sea Ice Extent - Northern Hemisphere (MASIE-NH), Version 1. Subset for June 2015., *NSIDC Natl. Snow Ice Data Center, Boulder, CO, USA*, doi:10.7265/N5GT5K3K. Available from: http://dx.doi.org/10.7265/N5GT5K3K (Accessed 21 March 2017)

Frieß, U., H. Sihler, R. Sander, D. Pöhler, S. Yilmaz, and U. Platt (2011), The vertical distribution of BrO and aerosols in the Arctic: Measurements by active and passive

differential optical absorption spectroscopy, *J. Geophys. Res. Atmos.*, *116*(D14), n/a--n/a, doi:10.1029/2011JD015938.

Halfacre, J. W. et al. (2014), Temporal and spatial characteristics of ozone depletion events from measurements in the Arctic, *Atmos. Chem. Phys.*, *14*(10), 4875–4894, doi:10.5194/acp-14-4875-2014.

Hausmann, M., and U. Platt (1994), Spectroscopic measurement of bromine oxide and ozone in the high Arctic during Polar Sunrise Experiment 1992, *J. Geophys. Res.*, *99*(D12), 25399–25413, doi:10.1029/94JD01314.

Holmes, C. D., D. J. Jacob, and X. Yang (2006), Global lifetime of elemental mercury against oxidation by atomic bromine in the free troposphere, *Geophys. Res. Lett.*, *33*(20), L20808, doi:10.1029/2006GL027176.

Holmes, C. D., D. J. Jacob, E. S. Corbitt, J. Mao, X. Yang, R. Talbot, and F. Slemr (2010), Global atmospheric model for mercury including oxidation by bromine atoms, *Atmos. Chem. Phys.*, *10*(24), 12037–12057, doi:10.5194/acp-10-12037-2010.

Hönninger, G., C. von Friedeburg, and U. Platt (2004), Multi axis differential optical absorption spectroscopy (MAX-DOAS), *Atmos. Chem. Phys.*, *4*(1), 231–254, doi:10.5194/acp-4-231-2004.

Huff, A. K., and J. P. D. Abbatt (2002), Kinetics and Product Yields in the Heterogeneous Reactions of HOBr with Ice Surfaces Containing NaBr and NaCl, *J. Phys. Chem. A*, *106*(21), 5279–5287, doi:10.1021/jp014296m.

Jacob, D. J. (2000), *Atmospheric Chemistry*, Princeton University Press, Princeton, New Jersey.

Johannessen, M., and A. Henriksen (1978), Chemistry of snow melt water: changes in concentration during melting, *Water Resour. Res.*, *14*(4), 615–619.

Kahan, T. F., N.-O. A. Kwamena, and D. J. Donaldson (2010a), Different photolysis kinetics at the surface of frozen freshwater vs. frozen salt solutions, *Atmos. Chem. Phys.*, *10*(22), 10917–10922, doi:10.5194/acp-10-10917-2010.

Kahan, T. F., R. Zhao, and D. J. Donaldson (2010b), Hydroxyl radical reactivity at the air-ice interface, *Atmos. Chem. Phys.*, *10*(2), 843–854, doi:10.5194/acp-10-843-2010.

Knepp, T. N. et al. (2010), Development of an autonomous sea ice tethered buoy for the study of ocean-atmosphere-sea ice-snow pack interactions: the O-buoy, *Atmos. Meas. Tech.*, *3*(1), 249–261, doi:10.5194/amt-3-249-2010.

Kwok, R. (2003), A study of the onset of melt over the Arctic Ocean in RADARSAT synthetic aperture radar data, *J. Geophys. Res.*, *108*(C11), 3363, doi:10.1029/2002JC001363.

Leser, H., G. Hönninger, and U. Platt (2003), MAX-DOAS Measurements of BrO and NO_2 in the Marine Boundary Layer, *Geophys. Res. Lett.*, *30*, 1537, doi:10.1029/2002GL015811.

Markus, T., J. C. Stroeve, and J. Miller (2009), Recent changes in Arctic sea ice melt onset, freezeup, and melt season length, *J. Geophys. Res.*, *114*(C12), C12024, doi:10.1029/2009JC005436.

McConnell, J. C., G. S. Henderson, L. Barrie, J. Bottenheim, H. Niki, C. H. Langford, and E. M. J. Templeton (1992), Photochemical bromine production implicated in Arctic boundary-layer ozone depletion, *Nature*, *355*(6356), 150–152.

Nghiem, S. V., and G. Neumann (2007), Arctic Sea-Ice Monitoring, in *2007 McGraw-Hill Yearbook of Science and Technology*, pp. 12–15, McGraw-Hill, New York.

Oltmans, S. J., and W. Komhyr (1986), Surface ozone distributions and variations from 1973 - 1984 measurements at the NOAA Geophysical Monitoring for Climate Change Baseline observatories, *J. Geophys. Res.*, *91*, 5229–5236.

Oltmans, S. J., R. C. Schnell, P. J. Sheridan, R. E. Peterson, S.-M. Li, J. W. Winchester, P. P. Tans, W. T. Sturges, J. D. Kahl, and L. A. Barrie (1989), Seasonal surface ozone and filterable bromine relationship in the high Arctic, *Atmos. Environ.*, *23*(11), 2431–2441, doi:10.1016/0004-6981(89)90254-0.

Oltmans, S. J., B. J. Johnson, and J. M. Harris (2012), Springtime boundary layer ozone depletion at Barrow, Alaska: Meteorological influence, year-to-year variation, and long-term change, *J. Geophys. Res.*, *117*(D14), D00R18, doi:10.1029/2011JD016889.

Perovich, D., J. A. Richter-Menge, B. Elder, T. Arbetter, K. Claffey, and C. Polashenski (2015), Observing and understanding climate change: Monitoring the mass balance, motion, and thickness of Arctic sea ice, Available from: http://imb-crrel-dartmouth.org/imb.crrel/ (Accessed 6 March 2017)

Peterson, P. K., W. R. Simpson, K. A. Pratt, P. B. Shepson, U. Frieß, J. Zielcke, U. Platt, S. J. Walsh, and S. V Nghiem (2015), Dependence of the vertical distribution of bromine monoxide in the lower troposphere on meteorological factors such as wind speed and stability, *Atmos. Chem. Phys.*, *15*(4), 2119–2137, doi:10.5194/acp-15-2119-2015.

Peterson, P. K. et al. (2017), Observations of Bromine Monoxide Transport In the Arctic Sustained on Aerosol Particles, *Atmos. Chem. Phys. Discuss.*, 1–20, doi:10.5194/acp-2016-

1141.

Platt, U., and G. Hönninger (2003), The role of halogen species in the troposphere, *Chemosphere*, *52*, 325–338.

Platt, U., and C. Janssen (1995), Observation and role of the free radicals NO3, ClO, BrO and IO in the troposphere, *Faraday Discuss.*, *100*, 175, doi:10.1039/fd9950000175.

Pöhler, D., L. Vogel, U. Frieß, and U. Platt (2010), Observation of halogen species in the Amundsen Gulf, Arctic, by active long-path differential optical absorption spectroscopy, *Proc. Natl. Acad. Sci.*, *107*(15), 6582–6587, doi:10.1073/pnas.0912231107.

Pratt, K. A. et al. (2013), Photochemical production of molecular bromine in Arctic surface snowpacks, *Nat. Geosci.*, *6*(5), 351–356, doi:10.1038/ngeo1779.

Richter, A., F. Wittrock, M. Eisinger, and J. P. Burrows (1998), GOME observations of tropospheric BrO in northern hemispheric spring and summer 1997, *Geophys. Res. Lett.*, *25*(14), 2683–2686, doi:10.1029/98GL52016.

Van Roozendael, M. et al. (2002), Intercomparison of BrO measurements from ERS-2 GOME, ground-based and balloon platforms, *Adv. Sp. Res.*, *29*(11), 1661–1666, doi:10.1016/S0273-1177(02)00098-4.

Schroeder, W. H., K. G. Anlauf, L. A. Barrie, J. Y. Lu, A. Steffen, D. R. Schneeberger, and T. Berg (1998), Arctic springtime depletion of mercury, *Nature*, *394*(6691), 331–332.

Sihler, H. et al. (2012), Tropospheric BrO column densities in the Arctic derived from satellite: retrieval and comparison to ground-based measurements, *Atmos. Meas. Tech.*, *5*(11), 2779–2807, doi:10.5194/amt-5-2779-2012.

Simpson, W. R., D. Carlson, G. Honninger, T. A. Douglas, M. Sturm, D. Perovich, and U. Platt (2007a), First-year sea-ice contact predicts bromine monoxide (BrO) levels at Barrow, Alaska better than potential frost flower contact, *Atmos. Chem. Phys.*, *7*(3), 621–627, doi:10.5194/acp-7-621-2007.

Simpson, W. R. et al. (2007b), Halogens and their role in polar boundary-layer ozone depletion, *Atmos. Chem. Phys.*, *7*(16), 4375–4418, doi:10.5194/acp-7-4375-2007.

Simpson, W. R., S. S. Brown, A. Saiz-Lopez, J. A. Thornton, and R. von Glasow (2015), Tropospheric Halogen Chemistry: Sources, Cycling, and Impacts, *Chem. Rev.*, *115*(10), 4035–4062, doi:10.1021/cr5006638.

Simpson, W. R. et al. (2017), Horizontal and vertical structure of reactive bromine events probed by bromine monoxide MAX-DOAS spectroscopy, *Atmos. Chem. Phys. Discuss.*, 1–29, doi:10.5194/acp-2017-187.

Steffen, A. et al. (2008), A synthesis of atmospheric mercury depletion event chemistry in the atmosphere and snow, *Atmos. Chem. Phys.*, *8*(6), 1445–1482, doi:10.5194/acp-8-1445-2008.

Stone, R. S., E. G. Dutton, J. M. Harris, and D. Longenecker (2002), Earlier spring snowmelt in northern Alaska as an indicator of climate change, *J. Geophys. Res. Atmos.*, *107*(D10), ACL 10-1-ACL 10-13, doi:10.1029/2000JD000286.

Taillandier, A.-S., F. Domine, W. R. Simpson, M. Sturm, T. A. Douglas, and K. Severin (2006), Evolution of the snow area index of the subarctic snowpack in central Alaska over a whole season. Consequences for the air to snow transfer of pollutants, *Environ. Sci. Technol.*, *40*(24), 7521–7527, doi:10.1021/es060842j.

Theys, N. et al. (2011), Global observations of tropospheric BrO columns using GOME-2 satellite data, *Atmos. Chem. Phys.*, *11*(4), 1791–1811, doi:10.5194/acp-11-1791-2011.

Vionnet, V., E. Brun, S. Morin, A. Boone, S. Faroux, P. Le Moigne, E. Martin, and J.-M. Willemet (2012), The detailed snowpack scheme Crocus and its implementation in SURFEX v7.2, *Geosci. Model Dev.*, *5*(3), 773–791, doi:10.5194/gmd-5-773-2012.

Wagner, T., and U. Platt (1998), Satellite mapping of enhanced BrO concentrations in the troposphere, *Nature*, *395*(6701), 486–490, doi:10.1038/26723.

Wennberg, P. (1999), Bromine explosion, *Nature*, *397*, 299–301.

Wever, N., C. Fierz, C. Mitterer, H. Hirashima, and M. Lehning (2014), Solving Richards Equation for snow improves snowpack meltwater runoff estimations in detailed multi-layer snowpack model, *Cryosph.*, *8*(1), 257–274, doi:10.5194/tc-8-257-2014.

Winebrenner, D. P., E. D. Nelson, R. Colony, and R. D. West (1994), Observation of melt onset on multiyear Arctic sea ice using the ERS 1 synthetic aperture radar, *J. Geophys. Res.*, *99*(C11), 22425, doi:10.1029/94JC01268.

Wren, S. N., D. J. Donaldson, and J. P. D. Abbatt (2013), Photochemical chlorine and bromine activation from artificial saline snow, *Atmos. Chem. Phys.*, *13*(19), 9789–9800, doi:10.5194/acp-13-9789-2013.

Table 1. Seasonal end dates (SED) and melt onset dates (MOD) for all sites and years. The IMB column has the name of the ice mass balance buoy. Latitude and longitude are in degrees, N and E being positive. The dates are local date at the time zone of the site, and the numerical day of year (doy) is listed in parentheses.

Site Year	IMB	Lat	Lon	SED (doy)	MOD (doy)	Note
Utqiaġvik 2012		71.32	-156.6	2012-May-15 (136)	2012-May-17 (138)	
Utqiaġvik 2013		71.32	-156.6	2013-May-20 (140)	2013-May-20 (140)	1
Utqiaġvik 2014		71.32	-156.6	2014-Apr-29 (119)	2014-Apr-30 (120)	
Utqiaġvik 2015		71.32	-156.6	2015-May-14 (134)	2015-May-16 (136)	2
Utqiaġvik 2016		71.32	-156.6	2016-May-07 (128)	2016-May-10 (131)	
O-Buoy 2 2011	2010F	74.24	-150.9	2011-Jun-12 (163)	2011-Jun-12 (163)	3
O-Buoy 4 2012		84.51	-28.9	2012-May-31 (152)	2012-May-31 (152)	
O-Buoy 6 2012		86.80	-4. 6	2012-Jun-08 (160)	2012-Jun-10 (162)	4
O-Buoy 10 2014	2013F	76.35	-150.6	2014-Jun-11 (162)	2014-Jun-13 (164)	5
O-Buoy 10 2015	2013F	77.76	-150.7	2015-May-18 (138)	2015-May-18 (138)	
O-Buoy 11 2015	2014I	77.20	-143.4	2015-May-18 (138)	2015-May-19 (139)	
O-Buoy 12 2015		75.83	-164.6	2015-May-16 (136)	2015-May-18 (138)	
O-Buoy 14 2016		77.02	-156.5	2016-May-15 (136)	2016-May-11 (132)	

Notes:
1) Used 3rd MOD for Utqiaġvik 2013
2) Did not count oscillations on May 11/12 for Utqiaġvik 2015
3) Did not count late May diurnal temperature oscillations for O-Buoy 2 2011
4) Used 2nd MOD for O-Buoy 6 2012
5) Did not count early May brief warming periods for O-Buoy 10 2014

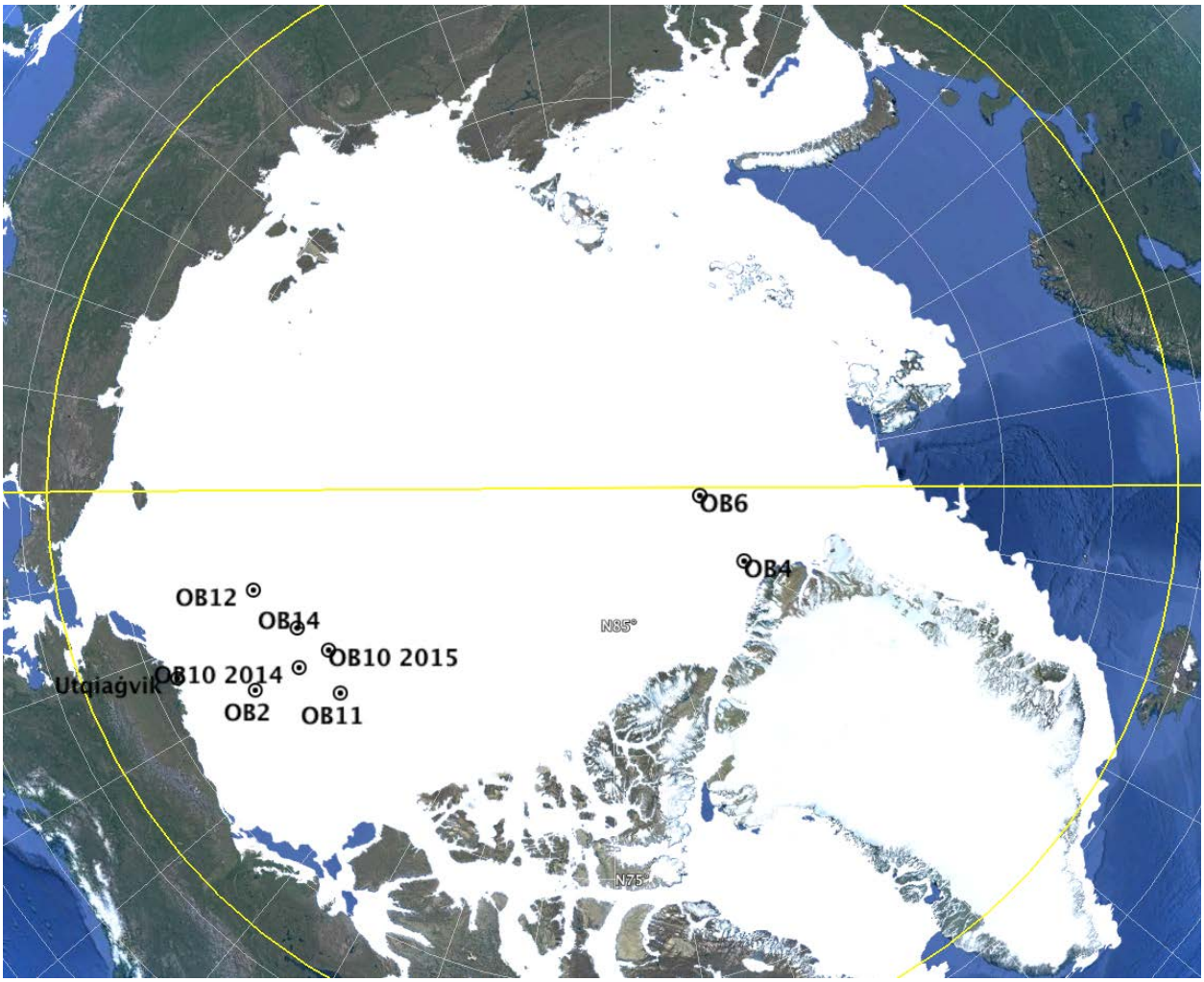

Figure 1. Locations sites used in this study overlaid on May 2015 MASIE [*Fetterer et al.*, 2010] sea ice extent data visualized in Google Earth. The O-Buoy locations are shown at the location of their seasonal end date, as listed in Table 1. The straight yellow line is 0° and 180° longitude and the yellow arc is the Arctic Circle.

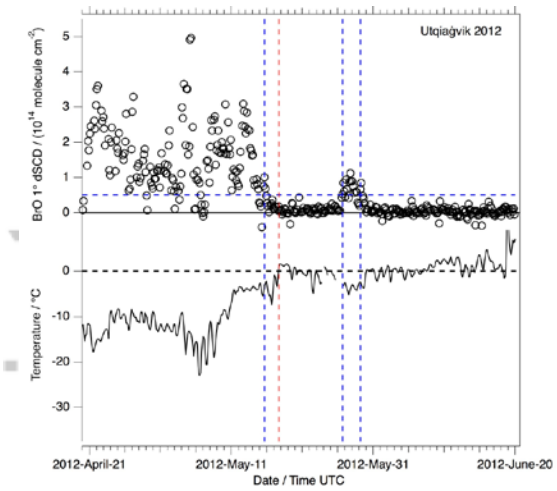

d vertical line = melt onset date

(MOD)

Figure 2. BrO 1° elevation dSCD (top panels) and air temperature (bottom panels) from April 20

– June 20 at Utqiaġvik from 2012—2016 averaged in 3-hour intervals. The BrO plot includes the threshold used for determining seasonal end date as a blue horizontal dashed line. Blue dashed vertical lines are located at termination and recurrence dates for BrO being above threshold. The horizontal black dashed line at 0°C is the threshold for melt onset. The red dashed vertical line is the melt onset date.

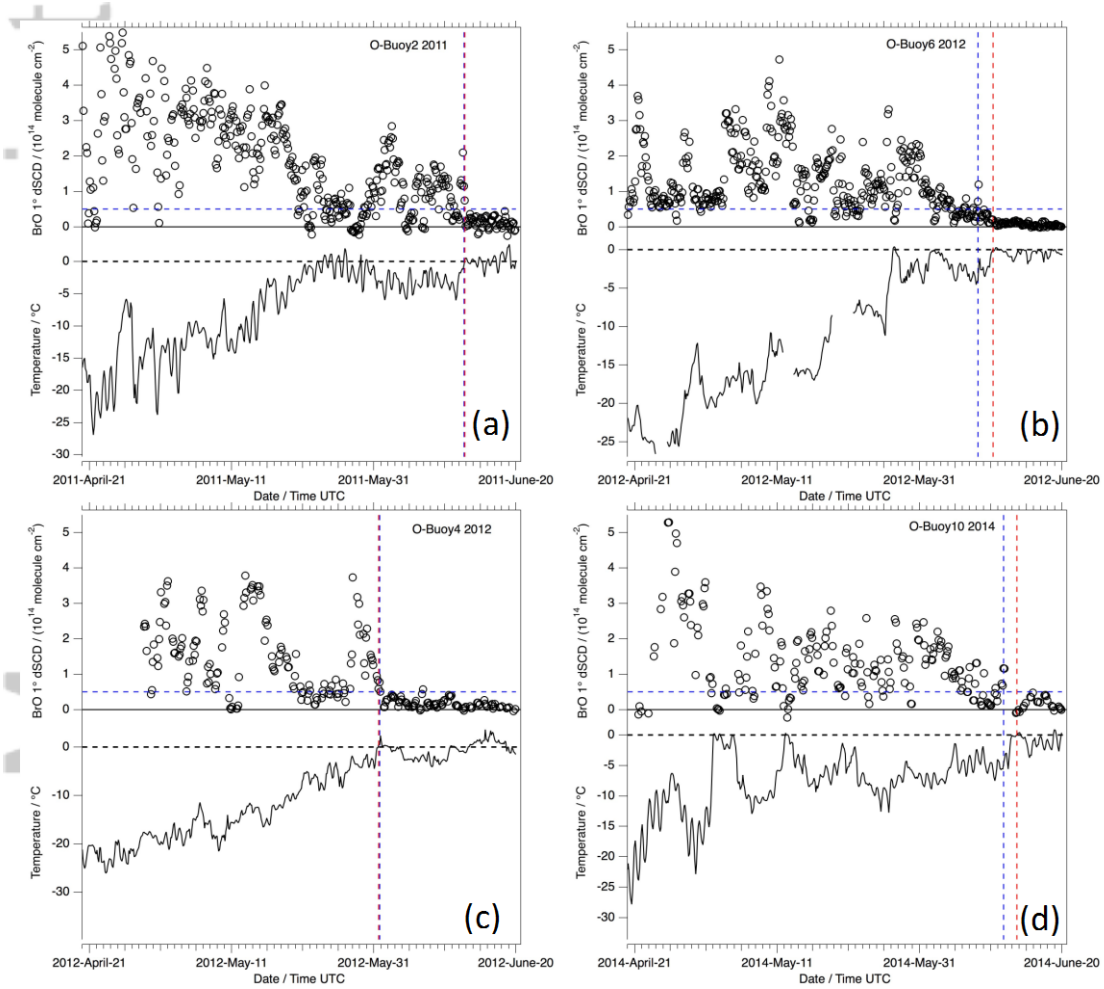

Figure 3. BrO 1° elevation dSCD (top panels) and air temperature (bottom panels) from four O-Buoy site/year combinations. The blue and black horizontal dashed lines are BrO and temperature thresholds, respectively. The blue dashed vertical lines are located at BrO termination and recurrence dates, and the red dashed vertical line is the melt onset date.

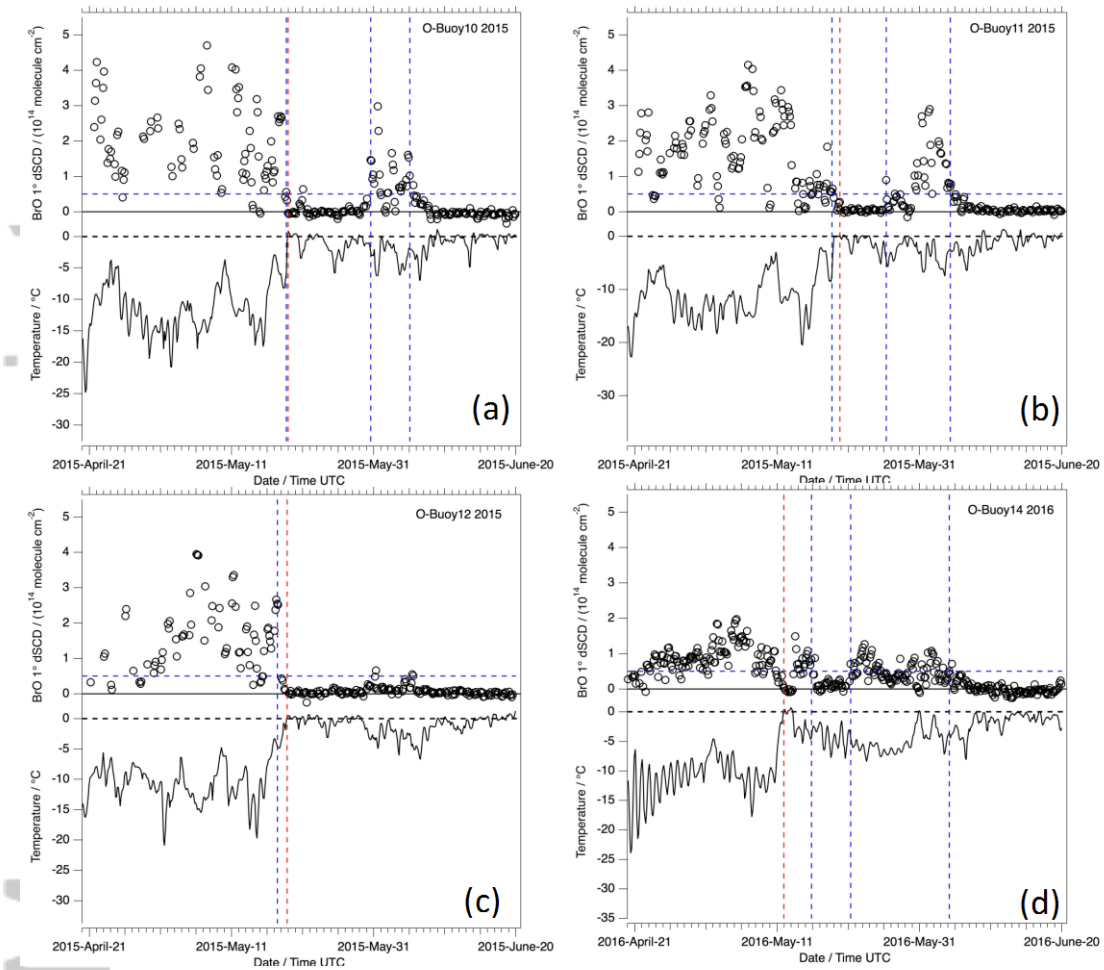

Figure 4. BrO 1° elevation dSCD (top panels) and air temperature (bottom panels) from four more O-Buoy site/year combinations. The blue and black horizontal dashed lines are BrO and temperature thresholds, respectively. The blue dashed vertical lines are located at BrO termination and recurrence dates, and the red dashed vertical line is the melt onset date.

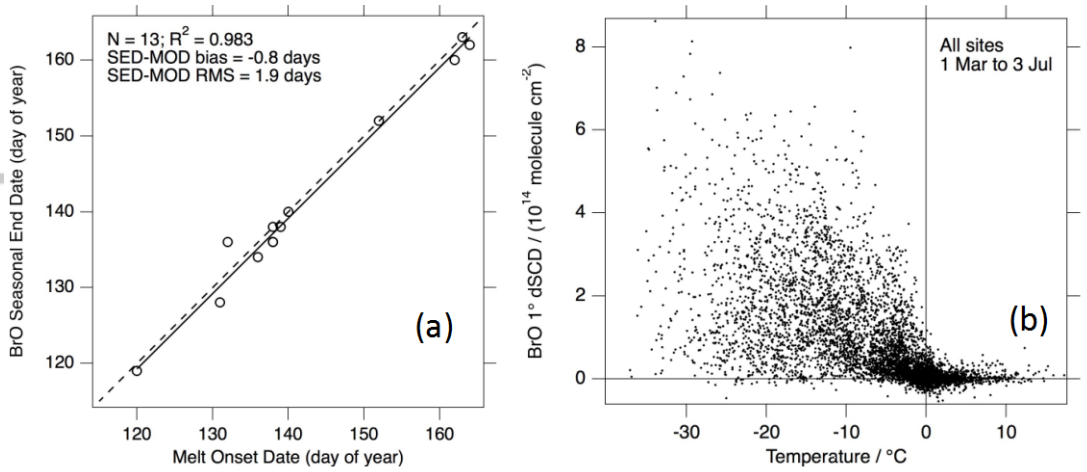

Figure 5. Panel (a) shows the correlation between the BrO seasonal end date and melt onset date. The black dashed line is the 1:1 line, and the solid line is the orthogonal distance regression (ODR) best fit line. Panel (b) shows the relationship between BrO 1° dSCD and ambient air temperature.

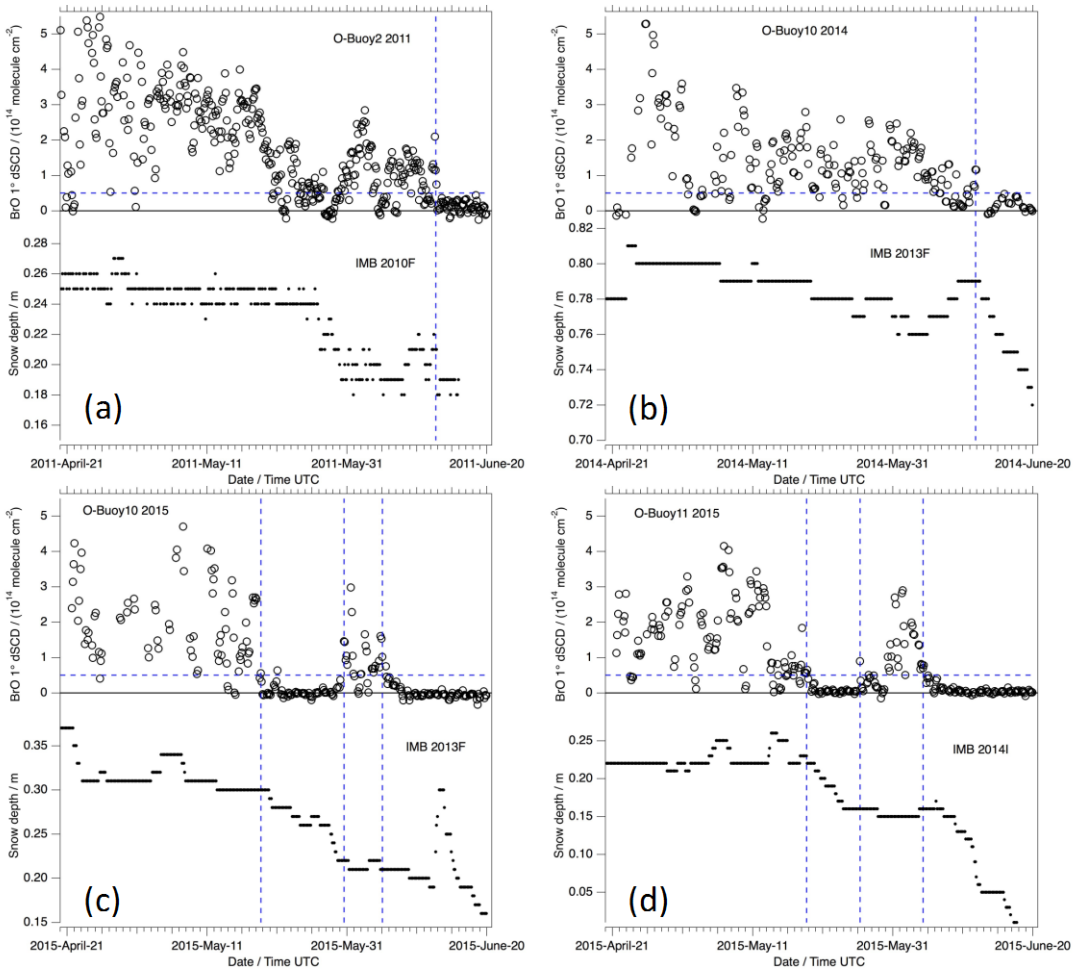

Figure 6. BrO 1° dSCD (top panel) and snow depth (bottom panel) for the four O-Buoys that were co-located with ice mass balance buoys (IMBs). The blue dashed lines indicate BrO termination and recurrence dates.

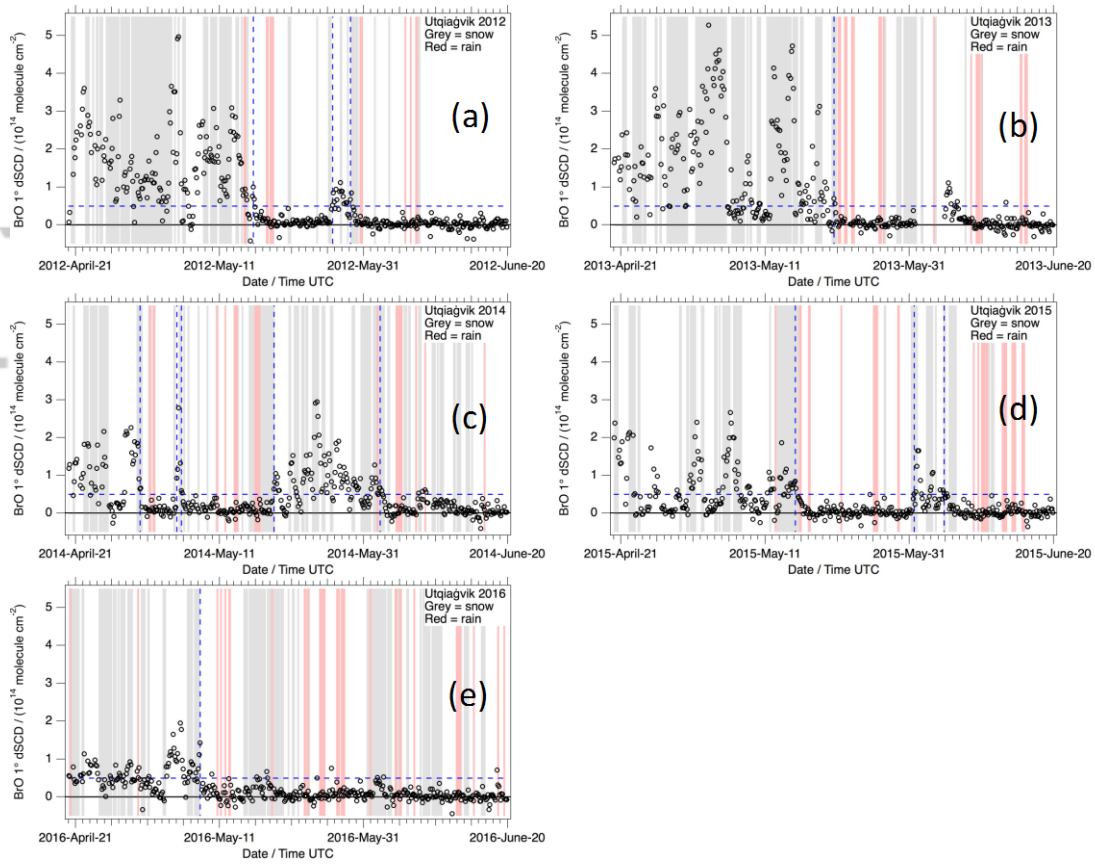

Figure 7. BrO 1° dSCD compared to precipitation observations from the Utqiaġvik airport (PABR). During each 3-hour interval, the grey background shading indicates >1 METAR code indicating snow, while red shading shows >1 METAR code indicating rain. The two early season rain events during 2016 were freezing rain events.

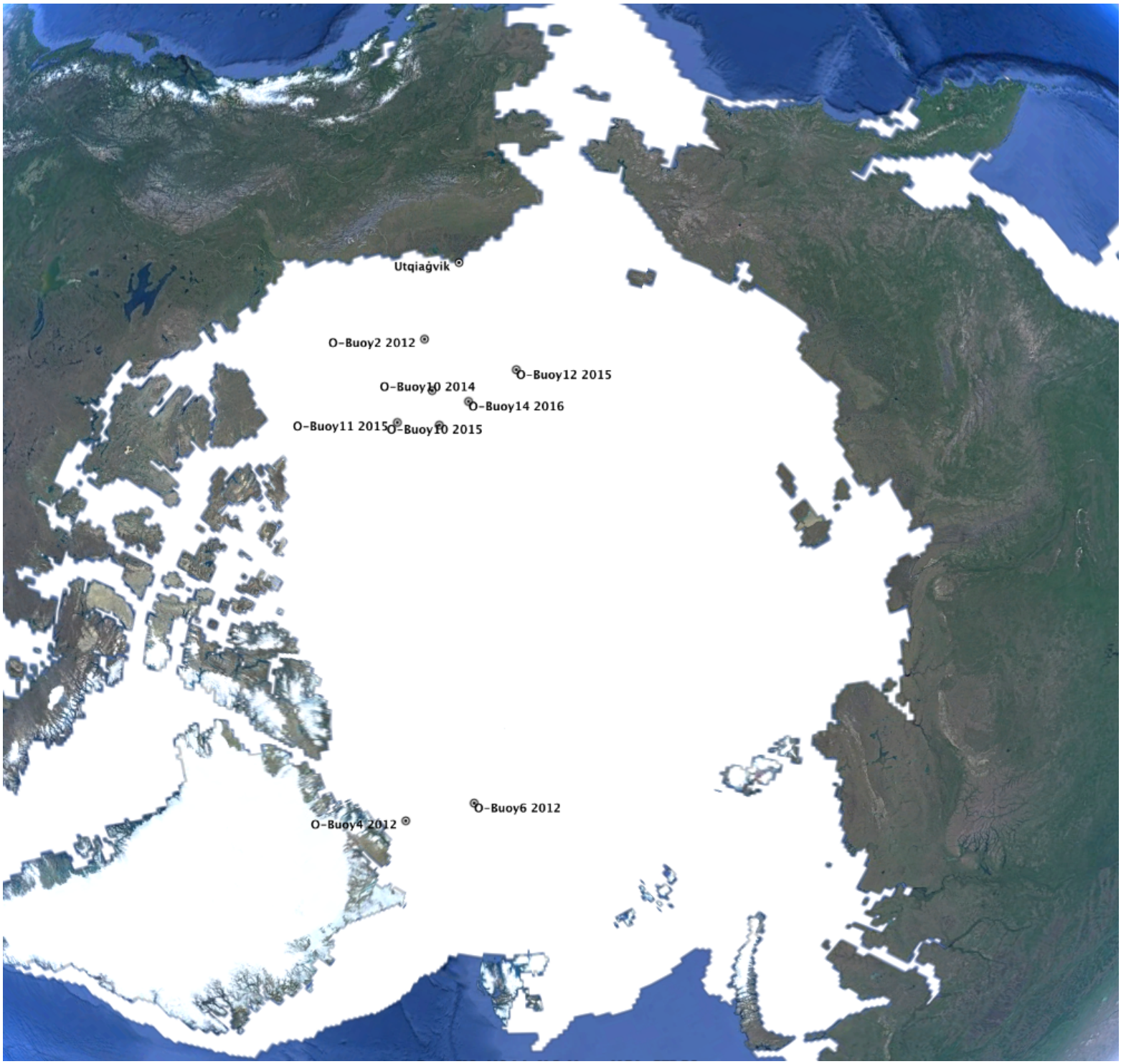

2017JD026906-f01-z-.tif

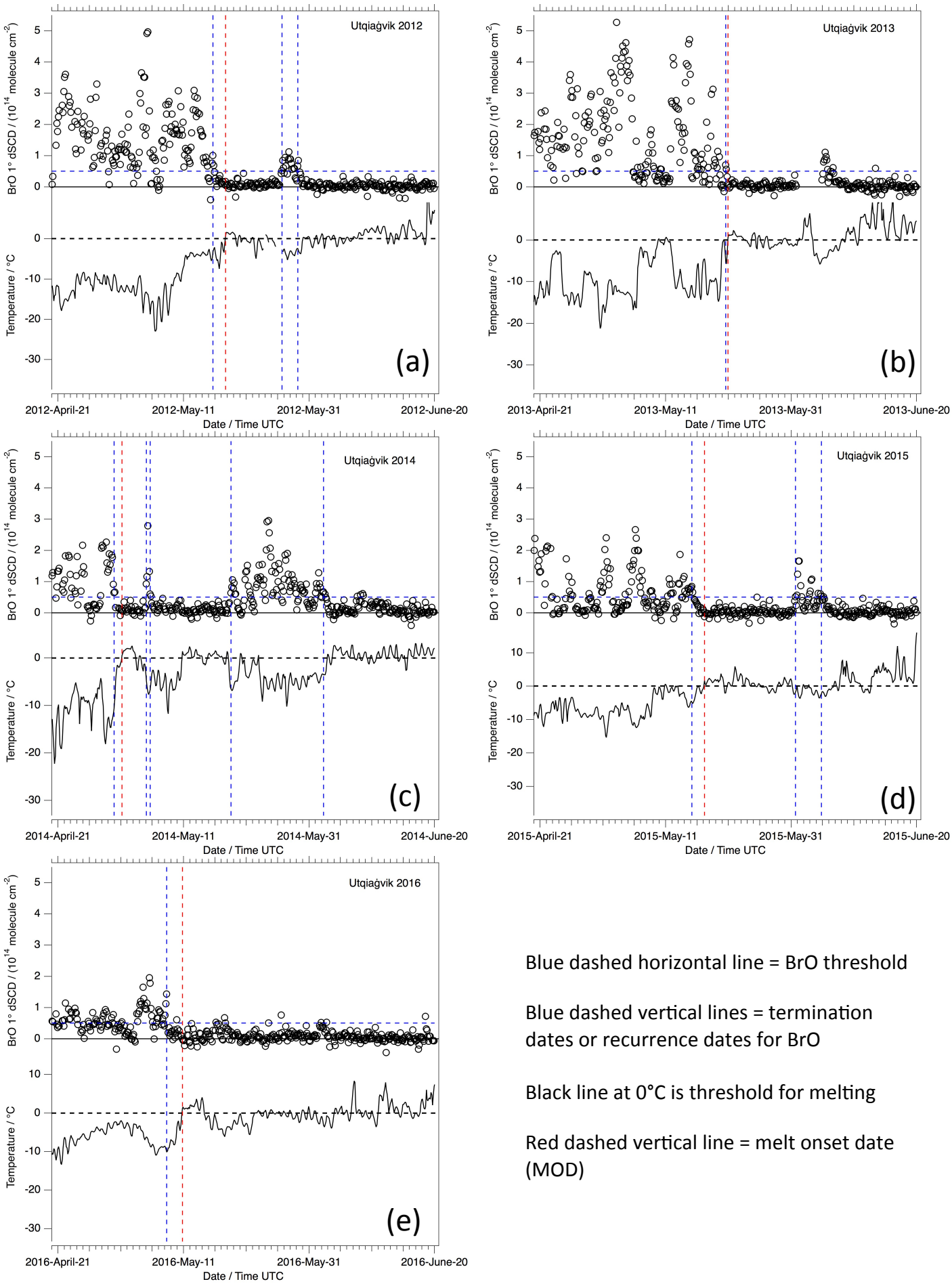

Blue dashed horizontal line = BrO threshold

Blue dashed vertical lines = termination dates or recurrence dates for BrO

Black line at 0°C is threshold for melting

Red dashed vertical line = melt onset date (MOD)